



Cite this: *Phys. Chem. Chem. Phys.*,  
2024, 26, 7611

# Substrate-induced strain and exchange field effects on the electronic and thermal properties of monolayer $\beta_{12}$ -borophene

Bui Dinh Hoi,<sup>a</sup> Le Thi Thu Phuong,<sup>a</sup> Pham Viet Dung<sup>b</sup> and  
Tran Cong Phong<sup>b,\*cd</sup>

The recently uncovered two-dimensional materials serve as versatile building blocks for electronic devices. In this study, we methodically investigate the impact of substrate-induced strain and exchange field effects on the electronic density of states (EDOS) and electronic heat capacity (EHC) of single-layer  $\beta_{12}$ -borophene. Utilizing the Green's function approach, we compute these functions. The van Hove singularities in EDOS are observed to shift with strain, and depending on the direction and strength of the exchange field, the number of singularities increases. All these responses can be attributed to the renormalization of the velocity of electronic bands. Additionally, the inherent Schottky anomaly (an unusual peak at low temperatures) in the EHC undergoes a notable shift to higher and lower temperatures and variations in the intensity of the EHC due to substrate effects.

Received 21st December 2023,  
Accepted 2nd February 2024

DOI: 10.1039/d3cp06225b

rsc.li/pccp

## 1 Introduction

In recent decades, the discovery of graphene<sup>1,2</sup> has led to the prominence of two-dimensional (2D) materials in the electronic industry. Despite graphene's unique features, its practical use is limited due to massless charge carriers, resulting in a gapless electronic band structure. To address this, various other 2D materials, such as silicene,<sup>3,4</sup> germanene,<sup>5</sup> stanene,<sup>6</sup> molybdenum disulfide,<sup>7,8</sup> and phosphorene,<sup>9,10</sup> have been introduced with couplings between spin and orbit and anisotropy structures, creating mass for electrons and a crucial gap for industrial applications like transistors.<sup>11,12</sup> These 2D materials exhibit remarkable properties compared to bulk materials,<sup>13,14</sup> making them promising for diverse applications across industries.

With a great attention to the world of 2D materials, borophene has emerged as a fascinating subject of study.<sup>15</sup> With its unique combination of Dirac-triplet fermions, showcasing its capacity to host two distinct types of charge carriers simultaneously, and diverse metallic phases, borophene is capturing the attention of both theoretical and experimental researchers.<sup>16–24</sup> This unique characteristic holds significant promise for electronic transport and adds a layer of complexity, but still useful, to

the electronic properties of materials.<sup>25–27</sup> Despite the metallic nature shared by most borophene allotropes, their electronic dispersions vary for different arrangement of atoms. Among the striped,  $\beta_{12}$ ,  $\chi_3$ , and honeycomb allotropes,  $\beta_{12}$ -borophene stands out as the most stable.<sup>28,29</sup>

Various methods can be employed to modify the characteristics of borophene. For instance, introducing an external perpendicular electric field has been demonstrated to create a gap, resulting in either an electron- or hole-doped semiconducting phase.<sup>30–33</sup> Adamska and Sharifzadeh utilized mechanical strain to manipulate the optical absorption spectrum.<sup>34</sup> Lherbier *et al.* explored the impact of oxidation on borophene's optical and electronic properties.<sup>35</sup> The influences of strain and surface functionalization on borophene's optical responses were also investigated.<sup>36</sup> A recent proposal suggests that the longitudinal (Hall) component of optical conductivity exhibits a redshift (blueshift) spectrum in the presence of an inversion symmetry-breaking field.<sup>37</sup> Simultaneously, the transverse optical conductivity demonstrates the coexistence of both redshift and blueshift spectra. Moreover, using first-principles calculations, it has been explored the routes to localize the carriers and open the band gap of borophene *via* chemical functionalization, ribbon construction, and defect engineering.<sup>38</sup> Another first principles density functional theory calculation has verified the directional dependency and found the tunable anisotropic behavior of the transport properties in  $\beta_{12}$ - and  $\chi$ -borophene polymorphs.<sup>39</sup>

To our knowledge, the substrate-induced effects on the electronic and thermal properties of  $\beta_{12}$ -borophene have not

<sup>a</sup> Faculty of Physics, University of Education, Hue University, Hue, 530000, Vietnam

<sup>b</sup> Nguyen Hue University, Dong Nai Province, Vietnam

<sup>c</sup> Atomic Molecular and Optical Physics Research Group, Institute for Advanced Study in Technology, Ton Duc Thang University, Ho Chi Minh City, Vietnam.  
E-mail: trancongphong@tdtu.edu.vn

<sup>d</sup> Faculty of Electrical and Electronics Engineering, Ton Duc Thang University, Ho Chi Minh City, Vietnam

been explored. This study, particularly focusing on the electronic density of states (EDOS) and electronic heat capacity (EHC) of Dirac-triplet fermions, aims to understand how the interaction between the  $\beta_{12}$ -borophene and a magnetic material as the substrate, which induces strain and exchange field to the host fermions, can affect the EDOS and EHC of  $\beta_{12}$ -borophene. The extent and nature of the strain depend on the differences in lattice parameters between the material and the substrate, while the strength and nature of the exchange field depends on the interface quality and the distance between the magnetic and host materials. It should be noted that, in our scenario, both strain and the exchange field originate from the influences exerted by the magnetic substrate. The exchange field arises from the magnetic moments of ions, whereas the strain effect is induced by the interaction between magnetic ions and host boron atoms. This interaction results in a direct deformation or alteration in the shape of both systems. We are not considering the growth process of borophene on the substrate. Instead, we place the grown and prepared borophene on a magnetic substrate such that in practical terms their states can interact and influence each other. The research delves into the control of van Hove singularities (both their height and number) through induced strain and exchange field, utilizing a tight-binding Hamiltonian model and the Green's function technique.

This paper is structured as follows. Section 2 focuses on the effective tight-binding Hamiltonian model of  $\beta_{12}$ -borophene in the absence and presence of magnetic substrate. Section 3 is dedicated to the exploration of the EDOS and EHC of  $\beta_{12}$ -borophene. Section 4 presents the results, and a comprehensive conclusion is provided in Section 5.

## 2 Tight-binding Hamiltonian model

To explore the EHC of  $\beta_{12}$ -borophene, it is crucial to monitor the behavior of the EDOS. Initially, a Hamiltonian model must be constructed to describe the states in EDOS. It is well-established that the electronic dispersion of graphene lattice arises from the orbital degrees of freedom along the  $z$  direction,

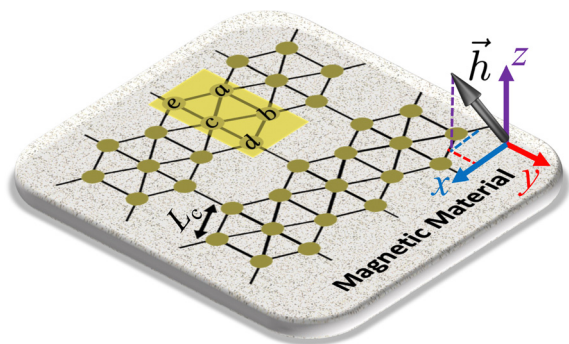


**Fig. 1** The structural configuration of  $\beta_{12}$ -borophene consists of five atoms, denoted as {a, b, c, d, e}, with a lattice constant of  $L_c \approx 2.926 \text{ \AA}$  on top of a magnetic substrate.<sup>25–27</sup> The shaded region outlines the rectangular unit cell. The substrate induces strain and exchange field  $\vec{h}$  to the boron atoms.

*i.e.*,  $p_z$ . Given the structural similarities between graphene and  $\beta_{12}$ -borophene, one expects that the electronic properties of  $\beta_{12}$ -borophene are predominantly influenced by the  $p_z$  orbitals of boron atoms.<sup>25–27</sup> For five atoms a, b, c, d, e in the unit cell of  $\beta_{12}$ -borophene and a lattice constant of  $L_c \approx 2.926 \text{ \AA}$ ,<sup>25–27</sup> as shown in Fig. 1, the proposed pristine model is as follows:

$$\mathcal{H}_0 = \sum_{\ell} \varepsilon_{\ell} c_{\ell}^{\dagger} c_{\ell} + \sum_{\ell k} t_{\ell k} c_{\ell}^{\dagger} c_k + \text{H.c.}, \quad (1)$$

where  $c_{\ell}^{\dagger}$  creates an electron at site  $\ell$ . Without the presence of the substrate, the pristine Hamiltonian is represented by a  $5 \times 5$  matrix, as follows:<sup>25</sup>

$$\mathcal{H}_0(\vec{k}) = \begin{pmatrix} \varepsilon_a & t_{ab}h_{12} & t_{ac}f_{\vec{k}}^* & 0 & t_{ae}f_{\vec{k}}^* \\ t_{ab}h_{12}^* & \varepsilon_b & t_{bc}h_{12} & t_{bd}f_{\vec{k}}^* & 0 \\ t_{ac}f_{\vec{k}}^* & t_{bc}h_{12}^* & \varepsilon_c & t_{cd}h_{12} & t_{ce}f_{\vec{k}}^* \\ 0 & t_{bd}f_{\vec{k}}^* & t_{cd}h_{12}^* & \varepsilon_d & t_{de}h_{12} \\ t_{ae}f_{\vec{k}}^* & 0 & t_{ce}f_{\vec{k}}^* & t_{de}h_{12}^* & \varepsilon_e \end{pmatrix}, \quad (2)$$

where  $\vec{k} = (k_x, k_y)$  represents the momentum,  $h_{12} = 2f_{\vec{k}} \cos(k_x L_c/2)$ ,  $t_{\ell k}$  denotes the hopping energy,  $\varepsilon_{\ell}$  stands for the on-site energy, and  $f_{\vec{k}} = \exp[ik_y L_c/2\sqrt{3}]$  according to previous works.<sup>25,26</sup> The hopping parameters leverage the inversion symmetry among boron atoms in  $\beta_{12}$ -borophene,<sup>26,30</sup> resulting in specific values:  $\varepsilon_a = \varepsilon_e = +0.196$ ,  $\varepsilon_b = \varepsilon_d = -0.058$ ,  $\varepsilon_c = -0.845$ ,  $t_{ab} = t_{de} = -2.04$ ,  $t_{ac} = t_{ce} = -1.79$ ,  $t_{bc} = t_{cd} = -1.84$ ,  $t_{bd} = -1.91$ , and  $t_{ae} = -2.12$  (all in units of eV).

When  $\beta_{12}$ -borophene is placed on top of a substrate, we move forward by inducing strain in the lattice of atoms, which includes orbital hybridization. The strain effect is induced by the interaction between magnetic ions and host boron atoms. This interaction results in a direct deformation or alteration in the shape of the substrate. It commonly involves varying bond lengths. This alteration, in turn, causes a modulation in the hopping energies  $t_{\ell k}$ .<sup>4,40,41</sup> Consequently, the strained Hamiltonian for  $\beta_{12}$ -borophene can be defined by substituting  $t_{\ell k} \rightarrow \tilde{t}_{\ell k}$ , where  $\tilde{t}_{\ell k}$  denotes the strain-induced hopping constants. In this context, the coordinates of unstrained atomic sites  $\ell$ , denoted as  $r_{\ell\alpha}$  for  $\alpha = x, y, z$ , undergo modulation due to strain, following  $r_{\ell\alpha} \rightarrow \tilde{r}_{\ell\alpha} = r_{\ell\alpha}(1 + \varepsilon_x)$ , where  $\varepsilon_x$  represents the strain modulus along the  $x$ -direction. Inspired by the Harrison rule<sup>42</sup> within a linear deformation regime ( $t_{\ell k} \propto 1/r_{\ell\alpha}^2$ ), the transformation is given by:

$$t_{\ell k} \rightarrow \tilde{t}_{\ell k} \approx t_{\ell k}(1 - 2\varepsilon_x). \quad (3)$$

It is worth noting that the dimensionless geometrical coefficients including the effects of buckling resulting from the application of strain (usually less than 1 and averaging 1/2 in our phenomenological model) are already accounted for in  $\varepsilon_x$ .<sup>40</sup> This modulation influences the electronic properties of  $\beta_{12}$ -borophene, yielding a new  $5 \times 5$  matrix for the Hamiltonian with  $\tilde{t}_{\ell k}$ .

The exchange field, however, arises from the magnetic moments of ions. In exploring the magnetic proximity effect,

the substrate is chosen to be a magnetic material characterized by magnetization,<sup>43–45</sup> as illustrated in Fig. 1:

$$\vec{h} = h(\sin \theta \cos \phi, \sin \theta \sin \phi, \cos \theta). \quad (4)$$

Here,  $h$  represents the strength of the exchange field, and  $\theta$  ( $\phi$ ) denotes the polar (azimuthal) angle with respect to the  $z$  axis and the  $x$ - $y$  plane. The interface between the two materials has the potential to induce magnetism in a non-magnetic material when near a magnetic counterpart. Consequently, this process leads to the renormalization of the velocities of bands. The in-plane vector potential for the induced exchange field  $h$  is represented by the gauge field  $\vec{A} = \left( \frac{h_y}{t_{lk}}, -\frac{h_x}{t_{lk}} \right)$ , and the following change is made to the momentum space of the system:

$$\tilde{k}_x^{lk} = k_x + \frac{h_y}{t_{lk}}, \quad (5a)$$

$$\tilde{k}_y^{lk} = k_y - \frac{h_x}{t_{lk}}. \quad (5b)$$

On the other hand, it is established that the exchange field along the  $z$  direction can be seamlessly integrated into the Hamiltonian as a mass term  $h_z$  in the diagonal elements. Nevertheless, owing to the inversion symmetry existing between {a and e} or {b and d} atoms (see Fig. 1), the influence of the substrate on the central c atoms is disregarded. This is because the wave functions of these atoms adequately cancel each other out in the final responses.

Thereby, the following Hamiltonian is achieved in the presence of the substrate-induced strain and exchange field effects:

$$\mathcal{H}(\vec{k}) = \begin{pmatrix} \varepsilon_a + h_z & \tilde{t}_{ab}h_{12} & \tilde{t}_{ac}f_k^* & 0 & \tilde{t}_{ae}f_k^* \\ \tilde{t}_{ab}h_{12}^* & \varepsilon_b + h_z & \tilde{t}_{bc}h_{12} & \tilde{t}_{bd}f_k^* & 0 \\ \tilde{t}_{ac}f_k^* & \tilde{t}_{bc}h_{12}^* & \varepsilon_c & \tilde{t}_{cd}h_{12} & \tilde{t}_{ce}f_k^* \\ 0 & \tilde{t}_{bd}f_k^* & \tilde{t}_{cd}h_{12}^* & \varepsilon_d - h_z & \tilde{t}_{de}h_{12} \\ \tilde{t}_{ae}f_k^* & 0 & \tilde{t}_{ce}f_k^* & \tilde{t}_{de}h_{12}^* & \varepsilon_e - h_z \end{pmatrix}. \quad (6)$$

### 3 Electronic density of states and heat capacity

Moving closer to the EDOS and EHC,<sup>46</sup> which are the main focuses of this paper, we compute the EDOS for  $\beta_{12}$ -borophene both in the absence and presence of the strain and exchange field.<sup>47</sup> To achieve this, we utilize the Green's function method, leveraging the Hamiltonian provided in eqn (6):

$$G(\vec{k}, \mathcal{E}) = \frac{1}{\mathcal{E} + i\eta - \mathcal{H}(\vec{k})}, \quad (7)$$

where the phenomenological energy factor  $\eta = 2$  meV serves as a tuning parameter regulating the visibility of singularities. The main origin of the energy factor  $\eta$  lies in the Matsubara frequency employed in Green's functions approach.<sup>47</sup> In this

context, the analytical continuation in the complex plane is achieved by transforming  $i\mathcal{E}$  to  $\mathcal{E} + i\eta$ . To derive EDOS, we start with the usual definition of DOS of a system, which is commonly described by  $\mathcal{D}(\mathcal{E}) = \sum_m \delta(\mathcal{E} - \mathcal{E}_m)$ ,<sup>48–51</sup> with  $\mathcal{E}_m$  being

the normalized eigenvalues supposed to be countable for simplicity with  $m$  counter ( $m = 1-5$  in our system). Using the definition of the Dirac delta function  $\delta(x) = \lim_{a \rightarrow 0} [a/\pi(x^2 + a^2)]$ ,

DOS can be quickly deduced as:

$$\mathcal{D}(\mathcal{E}) = -\frac{1}{\pi} \text{Tr} \sum_{\vec{k}} \text{Im} \frac{1}{\mathcal{E} + i\eta - \mathcal{H}(\vec{k})}. \quad (8)$$

Hence, the impact of the substrate and boron electrons' propagation on a particular place within the lattice is encompassed in the diagonal elements of eqn (7).

Subsequently, we continue with the computation of the EHC, which is commonly introduced when the heat is added to (or removed from) the material to change the temperature. In general, there are two mechanisms, phononic (from lattice degrees of freedom) and electronic (from charge degrees of freedom), influencing the thermal characteristics of matter in response to temperature changes. However, if the electron concentration is high, the charge contribution tends to be dominant. Therefore, EHC essentially focuses on the details of the charge excitations.<sup>52</sup> To achieve this, we initially determine the energy change at finite temperatures:

$$\Delta U = \int_0^\infty d\mathcal{E} \mathcal{E} \mathcal{D}(\mathcal{E}) f(\mathcal{E}, T) - \int_0^{\mathcal{E}_F} d\mathcal{E} \mathcal{E} \mathcal{D}(\mathcal{E}), \quad (9)$$

in which  $f(\mathcal{E}, T) = 1/[\exp(\mathcal{E}/k_B T) + 1]$  ( $k_B$  being the Boltzmann constant) represents the Fermi-Dirac distribution function, and  $\mathcal{D}(\mathcal{E})$  denotes the EDOS as given by eqn (8). The total number of electrons,  $N = \int_0^{\mathcal{E}_F} d\mathcal{E} \mathcal{D}(\mathcal{E})$ , facilitates the rewriting of the equation as follows:  $\Delta U = \left( \int_0^{\mathcal{E}_F} + \int_{\mathcal{E}_F}^\infty \right) d\mathcal{E} (\mathcal{E} - \mathcal{E}_F) \mathcal{D}(\mathcal{E}) f(\mathcal{E}, T) - \int_0^{\mathcal{E}_F} d\mathcal{E} (\mathcal{E} - \mathcal{E}_F) \mathcal{D}(\mathcal{E}) = \int_0^{\mathcal{E}_F} d\mathcal{E} (\mathcal{E} - \mathcal{E}_F) \mathcal{D}(\mathcal{E}) [f(\mathcal{E}, T) - 1] + \int_{\mathcal{E}_F}^\infty d\mathcal{E} (\mathcal{E} - \mathcal{E}_F) \mathcal{D}(\mathcal{E}) f(\mathcal{E}, T)$ . Consequently, the derivative with respect to temperature at  $\mathcal{E}_F = 0$  yields:<sup>53–57</sup>

$$C(T) = \int_{-\infty}^{+\infty} \mathcal{E} \mathcal{D}(\mathcal{E}) \frac{\partial f(\mathcal{E}, T)}{\partial T} d\mathcal{E}. \quad (10)$$

### 4 Results

Examining eqn (3), the strength of strain modulus on the host boron atoms gains significance, anticipating diverse electronic and thermal responses. In the following analysis, we only focus on the strain scenario: uniaxial strain and biaxial strain. Based on the previously discussed hopping energies and the inversion symmetry between boron atoms in  $\beta_{12}$ -borophene, similar responses are expected for individual uniaxial  $\varepsilon_x$  and  $\varepsilon_y$ . Moreover, we utilize  $\varepsilon_{xy} > 0$  to denote tensile strain and  $\varepsilon_{xy} < 0$  for compressive strain.

In Fig. 2, we present a comparison between pristine and strained  $\beta_{12}$ -borophene. The black curves near zero energy

indicate that the clean system exhibits a metal, characterized by a non-zero EDOS.<sup>25–27</sup> By calculating eqn (6), we identify nearly ten van Hove singularities (vHs) in the EDOS, providing accurate broadness and flatness for the electronic band. The height of vHs correlates with the overlap strength of atomic orbitals, with high (low) heights corresponding to weak (strong) orbital overlap for flat (curved) bands. Notably, the vHs at energy  $-2$  eV originates from triplet fermions, as it is established in ref. 25, 26 and 30, while Dirac fermions are responsible of the metallic phase at zero energy. Equipped with this understanding of the pristine lattice, we proceed to explore two strain scenarios mentioned above. The uniaxially strained EDOS results are illustrated by the other color lines for  $\beta_{12}$ -borophene in Fig. 2(a). In the case of uniaxial strain, the system stays metal (see the inset panel) with almost the same number of vHs in both valence and conduction bands, compared to the pristine case. This suggests a strong overlap between boron atoms themselves with uniaxial strain. As a result of the uniaxial strain effect, the electronic bands are narrowed and broadened with  $\epsilon_{x/y} > 0$  and  $\epsilon_{x/y} < 0$ . A similar analysis is applied to the biaxially strained EDOS, as shown in Fig. 2(b), but both compression and tension rates are higher compared to the uniaxial case. The modulation of the EDOS due to strain has been firmly established through first-principles studies.<sup>58</sup>

Turning to the EHC behavior, without substrate, the temperature dependency of EHC of  $\beta_{12}$ -borophene is illustrated by

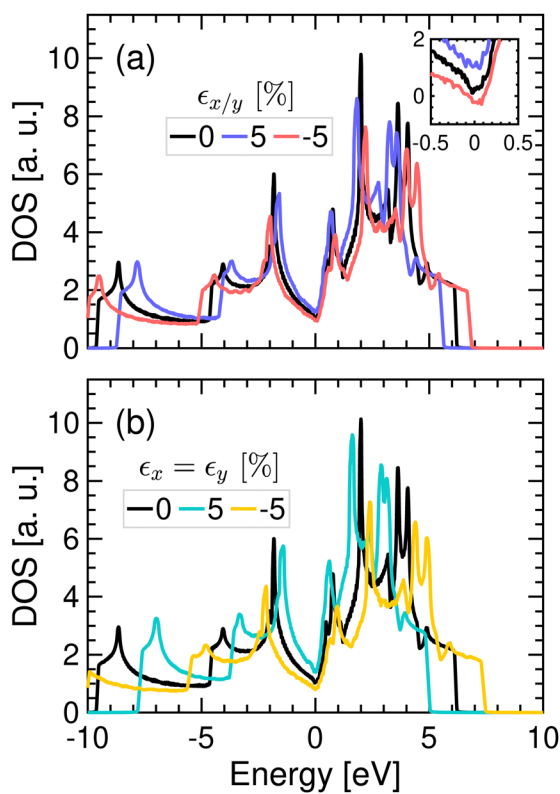


Fig. 2 The electronic density of states of  $\beta_{12}$ -borophene is depicted for (a) uniaxial and (b) biaxial strain scenarios. Broadening and narrowing the EDOS spectrum is a result of tensile and compressive strain, respectively.

the black line in Fig. 3 using the pristine tight-binding Hamiltonian. The EHC exhibits two inversely correlated acts at low and high temperatures, corresponding to the critical thermal energy  $k_B T_c \simeq 1$  eV, known as the Schottky anomaly. This anomaly is termed so because, under normal circumstances, heat capacity typically increases or remains constant with temperature,<sup>46</sup> whereas a solid's heat capacity has a peak at low temperatures. The critical temperature is explained by the fact that the probability of transition increases with temperature due to quantum effects at low temperatures, reaching a maximum at  $T_c$  when the states are filled. Beyond  $T_c$ , EHC starts to decrease with temperature due to a reduction in the probability of transition and the influence of thermal effects at higher temperatures.

With individual strain effect induced by the substrate, the Schottky anomaly undergoes a shift to lower (higher) thermal energies with tensile (compressive) strains – specifically, to 1.5 eV and 1.3 eV with tensile uniaxial and biaxial strains, respectively, and 0.7 eV and 0.6 eV with compressive uniaxial and biaxial strains. At the same time, although the intensity of the EHC increases with the compressive uniaxial and tensile biaxial strains, it decreases with the compressive biaxial and tensile uniaxial strains. The shift of  $T_c$  and increase/decrease of the EHC are attributed to the broadening and narrowing of the EDOS with compressive and tensile strains. As the temperature increases, thermal effects become dominant, causing all responses to converge, independent of the specific strain modulus.

Regarding the exchange field effect on EDOS, depicted by Fig. 4(a), an electron-doped semiconducting phase emerges. Notably, the minimal orbital overlap is specifically attributed to the higher conduction band as the height of vHs is higher than the valence band. In contrast to the earlier strain configuration, additional vHs are observed with  $h$ , dispersed across various energy levels. Likewise, there is also a sharp vHs at the conduction side providing a semi-flat electronic band. Apart from these changes, the whole spectrum is broadened with the

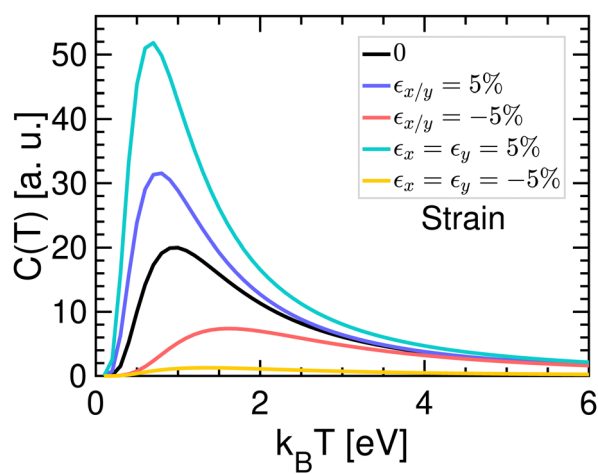


Fig. 3 Similar to Fig. 2, but depicting the strain effect on the EHC of  $\beta_{12}$ -borophene. The EHC is tuned when strain is applied, coinciding with the shift of the Schottky anomaly and increase/decrease of the EHC intensity.

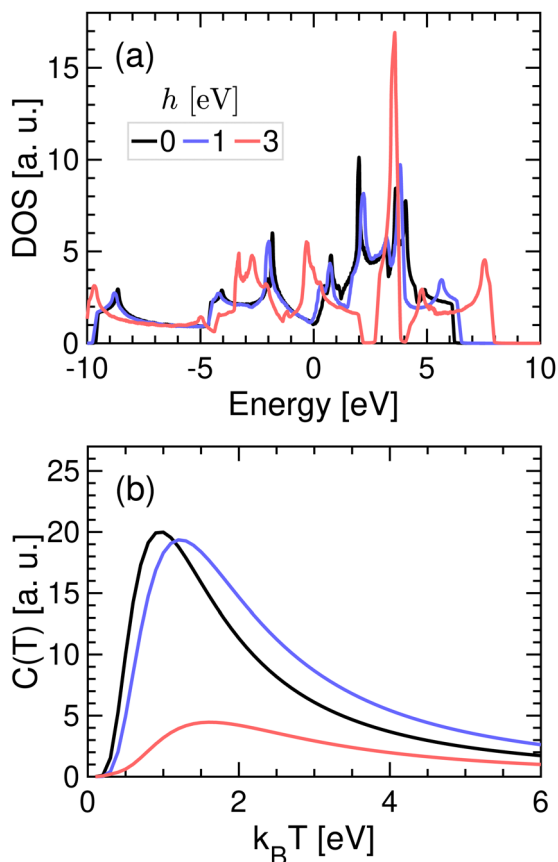


Fig. 4 Similar to Fig. 2, but for the exchange field effect on the (a) EDOS and (b) EHC of  $\beta_{12}$ -borophene. The Schottky anomaly experiences a shift with  $h$ , and the intensity of EHC is also increased (decreased) with weak (strong)  $h$ .

exchange field. In the presence of an exchange field along the directions  $\theta = 0$  and  $\phi = 0$ , as shown in Fig. 4(b), the EHC intensity experiences a decrease upon the application of the exchange field. The contribution from  $h = 1$  eV persists for the slight change of the EDOS. Intriguingly, our conclusion about the shift and the intensity of the Schottky anomaly at low temperatures holds such that  $T_c$  shifts to the higher thermal energies, and the height of its peak decreases with the exchange field due to the broadened EDOS.

To ensure a comprehensive analysis, we ultimately investigate the effect of the polar angle of the exchange field at  $h = 3$  eV and  $\phi = \pi/6$  on the EDOS and EHC of  $\beta_{12}$ -borophene. In Fig. 5(a), we observe qualitatively similar EDOS compared to the effect of the exchange field with zero angles, particularly the number of vHs. This suggests that the metallic phase of the system remains unresponsive to the direction of the exchange field. The primary reason for this behavior lies in the inversion symmetry of the Hamiltonian model, leading to the cancellation of overlapped orbitals along different directions. As a result of this, we again find a broadened electronic spectrum. It should be noted that  $\phi$  behaves in the same way and to avoid repetition, we have not included it in the present work.

As for the EHC behaviors with  $\theta$  under the same conditions, see Fig. 5(b), there is a nontrivial phenomenon where the EHC

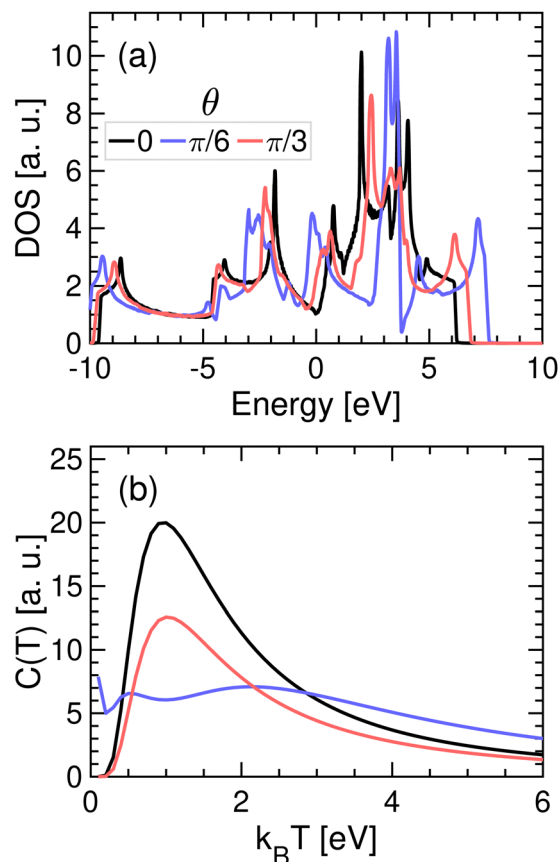


Fig. 5 The evolution of (a) EDOS and the (b) EHC of  $\beta_{12}$ -borophene with the direction of the substrate-induced exchange field.

begins with non-zero intensities at  $\theta = \pi/6$  rather than the expected zero intensity. Our analysis suggests that having both  $\theta$  and  $\phi$  equal to  $\pi/6$  contribute differently to the hopping parameters and it mainly can be attributed to role of {b and d} atoms in the model with smallest on-site energies. This implies that the probability of transition from the lowest energy states in the system at low temperatures remains high.

## 5 Summary

We have provided a comprehensive study for the effects of substrate-induced strain and exchange fields on the electronic density of states and electronic heat capacity of  $\beta_{12}$ -borophene using Green's function approach. Strain-induced shifts in the van Hove singularities and an increase in the number of singularities depending on the direction and strength of the exchange field are observed, attributed to the renormalization of electronic band velocities. The electronic heat capacity's Schottky anomaly experiences a notable temperature shift with substrate effects. Our work establishes that the sensitivity of the special fermions in  $\beta_{12}$ -borophene to substrate effects underscores the vital role of orbital hybridization in determining the physical properties of low-dimensional materials.

## Conflicts of interest

There are no conflicts to declare.

## Acknowledgements

This research is funded by Vietnam National Foundation for Science and Technology Development (NAFOSTED) under grant number 103.01-2021.68.

## References

- 1 K. S. Novoselov, A. K. Geim, S. V. Morozov, D. Jiang, Y. Zhang, S. V. Dubonos, I. V. Grigorieva and A. A. Firsov, *Science*, 2004, **306**, 666–669.
- 2 A. K. Geim, *Science*, 2009, **324**, 1530–1534.
- 3 C.-C. Liu, H. Jiang and Y. Yao, *Phys. Rev. B: Condens. Matter Mater. Phys.*, 2011, **84**, 195430.
- 4 B. D. Hoi, M. Yarmohammadi and H. A. Kazzaz, *J. Magn. Magn. Mater.*, 2017, **439**, 203–212.
- 5 M. Derivaz, D. Dentel, R. Stephan, M.-C. Hanf, A. Mehdaoui, P. Sonnet and C. Pirri, *Nano Lett.*, 2015, **15**, 2510–2516.
- 6 F.-f Zhu, W.-j Chen, Y. Xu, C.-l Gao, D.-d Guan, C.-h Liu, D. Qian, S.-C. Zhang and J.-f Jia, *Nat. Mater.*, 2015, **14**, 1020–1025.
- 7 A. Splendiani, L. Sun, Y. Zhang, T. Li, J. Kim, C.-Y. Chim, G. Galli and F. Wang, *Nano Lett.*, 2010, **10**, 1271–1275.
- 8 J. Yuan, Y. Chen, Y. Xie, X. Zhang, D. Rao, Y. Guo, X. Yan, Y. P. Feng and Y. Cai, *Proc. Natl. Acad. Sci. U. S. A.*, 2020, **117**, 6362–6369.
- 9 H. Liu, A. T. Neal, Z. Zhu, Z. Luo, X. Xu, D. Tománek and P. D. Ye, *ACS Nano*, 2014, **8**, 4033–4041.
- 10 H. Bui and M. Yarmohammadi, *J. Magn. Magn. Mater.*, 2018, **465**, 646–650.
- 11 J. Qiao, X. Kong, Z.-X. Hu, F. Yang and W. Ji, *Nat. Commun.*, 2014, **5**, 4475.
- 12 A. Castellanos-Gomez, L. Vicarelli, E. Prada, J. O. Island, K. L. Narasimha-Acharya, S. I. Blanter, D. J. Groenendijk, M. Buscema, G. A. Steele, J. V. Alvarez, H. W. Zandbergen, J. J. Palacios and H. S. J. van der Zant, *2D Mater.*, 2014, **1**, 025001.
- 13 W. Zhang, Y. Cui, C. Zhu, B. Huang, Y. Lou and S. Yan, *Mater. Chem. Phys.*, 2023, **305**, 127964.
- 14 C. Huan, P. Wang, B. He, Y. Cai and Q. Ke, *2D Mater.*, 2022, **9**, 045014.
- 15 P. Ranjan, J. M. Lee, P. Kumar and A. Vinu, *Adv. Mater.*, 2020, **32**, 2000531.
- 16 C. Özdoğan, S. Mukhopadhyay, W. Hayami, Z. B. Güvenc, R. Pandey and I. Boustani, *J. Phys. Chem. C*, 2010, **114**, 4362–4375.
- 17 I. Boustani, *Surf. Sci.*, 1997, **370**, 355–363.
- 18 M. H. Evans, J. D. Joannopoulos and S. T. Pantelides, *Phys. Rev. B: Condens. Matter Mater. Phys.*, 2005, **72**, 045434.
- 19 H. Tang and S. Ismail-Beigi, *Phys. Rev. Lett.*, 2007, **99**, 115501.
- 20 X. Wu, J. Dai, Y. Zhao, Z. Zhuo, J. Yang and X. C. Zeng, *ACS Nano*, 2012, **6**, 7443–7453.
- 21 E. S. Penev, S. Bhowmick, A. Sadrzadeh and B. I. Yakobson, *Nano Lett.*, 2012, **12**, 2441–2445.
- 22 H. Liu, J. Gao and J. Zhao, *Sci. Rep.*, 2013, **3**, 3238.
- 23 Y. Liu, E. S. Penev and B. I. Yakobson, *Angew. Chem., Int. Ed.*, 2013, **52**, 3156–3159.
- 24 Z. Zhang, Y. Yang, G. Gao and B. I. Yakobson, *Angew. Chem., Int. Ed.*, 2015, **54**, 13022–13026.
- 25 M. Ezawa, *Phys. Rev. B*, 2017, **96**, 035425.
- 26 B. Feng, O. Sugino, R.-Y. Liu, J. Zhang, R. Yukawa, M. Kawamura, T. Iimori, H. Kim, Y. Hasegawa, H. Li, L. Chen, K. Wu, H. Kumigashira, F. Komori, T.-C. Chiang, S. Meng and I. Matsuda, *Phys. Rev. Lett.*, 2017, **118**, 096401.
- 27 X. Zhang, J. Hu, Y. Cheng, H. Y. Yang, Y. Yao and S. A. Yang, *Nanoscale*, 2016, **8**, 15340–15347.
- 28 B. Feng, J. Zhang, Q. Zhong, W. Li, S. Li, H. Li, P. Cheng, S. Meng, L. Chen and K. Wu, *Nat. Chem.*, 2016, **8**, 563–568.
- 29 B. Feng, J. Zhang, R.-Y. Liu, T. Iimori, C. Lian, H. Li, L. Chen, K. Wu, S. Meng, F. Komori and I. Matsuda, *Phys. Rev. B*, 2016, **94**, 041408.
- 30 P. T. T. Le, T. C. Phong and M. Yarmohammadi, *Phys. Chem. Chem. Phys.*, 2019, **21**, 21790–21797.
- 31 B. D. Hoi, L. V. Tung, P. T. Vinh, D. Q. Khoa and L. T. T. Phuong, *Phys. Chem. Chem. Phys.*, 2021, **23**, 2080–2087.
- 32 H. T. T. Nguyen, B. D. Hoi, T. V. Vu, P. V. Nham and N. T. T. Binh, *Phys. Chem. Chem. Phys.*, 2020, **22**, 6318–6325.
- 33 D. Q. Khoa, N. N. Hieu and B. D. Hoi, *Phys. Chem. Chem. Phys.*, 2020, **22**, 286–294.
- 34 L. Adamska and S. Sharifzadeh, *ACS Omega*, 2017, **2**, 8290–8299.
- 35 A. Lherbier, A. R. Botello-Méndez and J.-C. Charlier, *2D Mater.*, 2016, **3**, 045006.
- 36 A. Mogulkoc, Y. Mogulkoc, D. Kecik and E. Durgun, *Phys. Chem. Chem. Phys.*, 2018, **20**, 21043–21050.
- 37 L. T. T. Phuong, B. D. Hoi and M. Yarmohammadi, *Phys. Rev. B*, 2022, **106**, 195409.
- 38 A. A. Kistanov, Y. Cai, K. Zhou, N. Srikanth, S. V. Dmitriev and Y.-W. Zhang, *Nanoscale*, 2018, **10**, 1403–1410.
- 39 V. Shukla, A. Grigoriev, N. K. Jena and R. Ahuja, *Phys. Chem. Chem. Phys.*, 2018, **20**, 22952–22960.
- 40 M. Yarmohammadi, B. D. Hoi and L. T. T. Phuong, *Sci. Rep.*, 2021, **11**, 3716.
- 41 M. Yarmohammadi, M. M. Nobahari, T. S. Tien and L. T. T. Phuong, *J. Phys.: Condens. Matter*, 2020, **32**, 465301.
- 42 W. Harrison, *Elementary Electronic Structure*, World Scientific, 1999.
- 43 M. Ezawa, *Phys. Rev. B: Condens. Matter Mater. Phys.*, 2014, **89**, 195413.
- 44 T. Yokoyama, *New J. Phys.*, 2014, **16**, 085005.
- 45 Y. Ando and L. Fu, *Annu. Rev. Condens. Matter Phys.*, 2015, **6**, 361–381.
- 46 A. Tari, *The Specific Heat of Matter at Low Temperatures*, Imperial College Press, 2003.
- 47 G. Mahan, *Many-Particle Physics*, Springer US, 2000.

- 48 R. Chegel, S. Behzad, Y. Wang and J. Xu, *Solid State Sci.*, 2021, **121**, 106737.
- 49 R. Chegel and S. Behzad, *Synth. Met.*, 2020, **266**, 116476.
- 50 H. Bui and M. Yarmohammadi, *Phys. E*, 2018, **103**, 76–80.
- 51 H. Bui and M. Yarmohammadi, *Superlattices Microstruct.*, 2018, **122**, 453–460.
- 52 C. Kittel, *Introduction to Solid State Physics*, Wiley, 2004.
- 53 R. Chegel, *J. Mol. Graphics Modell.*, 2023, **121**, 108372.
- 54 R. Chegel, *Phys. B*, 2022, **638**, 413921.
- 55 M. Yarmohammadi, *Phys. Lett. A*, 2017, **381**, 1261–1267.
- 56 M. Yarmohammadi, *Solid State Commun.*, 2017, **250**, 84–91.
- 57 M. Yarmohammadi, *J. Magn. Magn. Mater.*, 2016, **417**, 208–213.
- 58 B. Mortazavi, O. Rahaman, A. Dianat and T. Rabczuk, *Phys. Chem. Chem. Phys.*, 2016, **18**, 27405–27413.